Vietnam Journal of Science and Technology ***62*** *(3) (2024) 508-520*

doi:10.15625/2525-2518/17639

A high-sensitivity hydrogen gas sensor based on Ag nanoparticle-decorated porous Co_3O_4 nanorods

Vu Hung Sinh[1], Duong Tuan Quang[1], Tran Quy Phuong[2], Tran Thai Hoa[2], Nguyen Van Hieu[3], Nguyen Duc Cuong[1, 2, *]

[1]*University of Education, Hue University, 34 Le Loi, Hue City, Thua Thien Hue Province, Viet Nam*

[2]*University of Sciences, Hue University, 77 Nguyen Hue, Hue City, Thua Thien Hue Province, Viet Nam*

[3]*Faculty of Electrical and Electronic Engineering, Phenikaa University, Yen Nghia Ward, Ha Dong District, Hanoi city, Viet Nam*

[*]Emails: *nguyenduccuong@hueuni.edu.vn*

Received: 8 November 2022; Accepted for publication: 25 December 2023

Abstract. In this report, Ag nanoparticle-decorated cobalt carbonate hydroxide microflowers were synthesized using a simple hydrothermal approach without using surfactants, which were used as precursors to prepare Ag nanoparticle-decorated porous Co_3O_4 nanorods through an annealing process. The porous Co_3O_4 nanorods were composed of small primary nanoparticles with a size of ~ 10 nm, and their surface was decorated with uniform Ag nanoparticles (~ 10 nm). Sensors based on the porous Co_3O_4 nanorods decorated with Ag nanoparticles have higher sensitivity and selectivity to H_2 gas than other reduced gases, as well as rapid response-recovery times. The enhanced H_2 sensing properties of the sample may be attributed to the excellent catalytic features of Ag nanoparticles and unique porous Co_3O_4 nanorods. The results demonstrated the potential of Ag nanoparticle-decorated porous Co_3O_4 nanorods as sensing materials for the detection of hydrogen gas at low temperatures.

Keywords: Ag nanoparticles, porous Co_3O_4 nanorods, H_2, gas sensors.

Classification numbers: 2.4.4, 2.10.2.

1. INTRODUCTION

Metal oxide semiconductors (MOS), which include p-type and n-type semiconductors, have been considered promising sensing materials for the detection of toxics and flammable gases. This is owing to their fascinating advantages such as low cost, good stability, good repeatability and high response, rapid response-recovery times, and easy integration [1]. Until now, n-type metal oxide semiconductor-based sensors have been widely investigated, whereas the gas sensing properties of p-type metal oxide semiconductors have received less attention [2]. Recent reports indicated that p-type metal oxide semiconductor-based sensors have distinct merits such as low working temperature, good selectivity, good anti-humidity feature, and high thermal

stability [3]. Therefore, the development of p-type MOSs-based sensing materials to explore their new gas sensing performance is very necessary.

Among many p-type MOSs, cobalt oxide (Co_3O_4) with an indirect band gap of about 1.6-2.2 eV is of special interest owing to its potential applications such as catalysts, magnetic materials, in particular gas sensors, due to their excellent catalytic properties, multivalent characteristics and abundant adsorbed oxygen [4]. Wen *et al*. [5] synthesized rhombus-shaped Co_3O_4 nanorod arrays-based sensors that showed the highest sensitivity to ethanol because of good contact, porous structure, good crystallinity, high surface-to-volume ratio and open space. Geng *et al*. [6] reported that the Co_3O_4 nanosheets showed superior sensitivity to CO and CH_4 at room temperature, as well as good reproducibility and fast response/recovery times. Hoa *et al*. [7] indicated that the meso- and macroporous Co_3O_4 nanorods-based sensors showed high response and selectivity to acetone with fast response-recovery times. Many synthetic strategies have been developed to prepare Co_3O_4 nanostructures. Among them, the $Co(CO_3)_{0.5}(OH)\cdot 0.11H_2O$ nanostructure, which was an important candidate for various areas [8], has been considered a potential precursor for designing porous Co_3O_4 nanostructures. Recently, we have synthesized Co_3O_4 nanochains that showed good detection of H_2S with high sensitivity and rapid response time [9]. However, there are few reports on the H_2 gas sensing properties of Co_3O_4 nanostructures-based sensors.

Hydrogen is being investigated as a sustainable energy carrier because of its high energy density and environmental benignity. In addition, hydrogen is employed in numerous industrial fields, such as metallurgy, glass, electronics, chemicals, and the production of textile fibers [10]. However, H_2 is a flammable and explosive gas, which becomes explosive when its concentration increases beyond 4 %. [7]. Therefore, to avoid an explosion, it is essential to develop novel sensors with high sensitivity and rapid response-recovery times to monitor and detect hydrogen at low concentrations.

The use of noble metal nanoparticles such as Pd, Au and Ag decoration on the MOS nanostructures is a potential route to improving their H_2 gas sensing performance due to the catalytic effect of noble metal nanoparticles [11]. For example, the homogeneous and optimal distribution of the p-type PdO nanoparticles in n-type WO_3 film sensors demonstrated high sensitivity and low detection limit toward H_2 gas at 160 ^oC [12]. The Pd modified SnO_2 nanoparticles sensors remarkably upgraded the H_2 sensing performances compared with the pristine SnO_2 gas sensor, which could originate from the catalytic effect and resistance modulation [13]. The Pd-WO_3 nanoparticle sensors could detect H_2 at room temperature with a remarkably high response and selectivity [14]. The Ag-decorated ZnO nanocrystallines possessed excellent H_2 gas-sensing properties with a high gas response, fast response-recovery times, good repeatability and stability owing to the catalytic activity of Ag nanoparticles, which led to more active sites for the reaction of hydrogen on the surface of sensors [15]. Among noble metals, silver is the cheapest. Therefore, the Ag nanoparticle-decorated MOSs have been considered an effective method for designing novel sensing materials for detecting H_2 gas at lower cost.

In this report, we used a template-free hydrothermal approach for fabricating $Co(CO_3)_{0.5}(OH)\cdot 0.11H_2O$ microflowers, which were assembled by many nanorods. The microflowers obtained were decorated with Ag nanoparticles by the chemical reduction of Ag^+ ions using $NaBH_4$. As a result, the Ag-decorated $Co(CO_3)_{0.5}(OH)\cdot 0.11H_2O$ microflowers were annealed in air to form Ag-loaded porous Co_3O_4 nanorods. Gas sensing characteristics of as-synthesized nanomaterials showed that the Ag-decorated porous Co_3O_4 nanorods exhibited high response toward H_2, with selectivity and fast response-recovery times.

2. MATERIALS AND METHODS

2.1. Materials

Cobalt nitrate ($Co(NO_3)_2{\cdot}6H_2O$, silver nitrate ($AgNO_3$) and urea ($CO(NH_2)_2$ were purchased from Sigma-Aldrich. All reagents were of analytical grade and used without further purification.

2.2. Synthesis of Ag nanoparticles-decorated porous Co_3O_4 nanorods

Ag-decorated porous Co_3O_4 nanorods were fabricated via a simple and scalable hydrothermal method without using templates. First, $Co(CO_3)_{0.5}(OH){\cdot}0.11H_2O$ microflowers were synthesized using a slightly modified protocol of our recent report [9]. In a typical experiment, urea (0.075 mol) and $Co(No_3)_2{\cdot}6H_2O$ (0.001 mol) were added to 70 mL of deionized water, followed by stirring for 20 min to form a clear solution. This solution was transferred to a 100 mL Teflon-lined stainless steel autoclave. The autoclave was aged at 60 ◦C for 12 h, and then the reaction temperature was raised to and kept at 90 ◦C for 8 h. The $Co(CO_3)_{0.5}(OH){\cdot}0.11H_2O$ microflower sample was collected by centrifugation, and washed with distilled water and ethanol several times, and finally dried at 60 ◦C for 24 h. To decorate the $Co(CO_3)_{0.5}(OH){\cdot}0.11H_2O$ microflowers with Ag nanoparticles, 1 g of cobalt carbonate hydroxide microflowers was dissolved in 70 mL of DI. Then, 2 mL of 1 % $AgNO_3$ solution was added to this suspension, followed by stirring for 30 min. After that, 2 mL of 0.2 % $NaBH_4$ solution was slowly added to the above mixture, which was then stirred for 3 h. The products were collected by centrifugation and washed with distilled water and ethanol several times. The Ag nanoparticles-decorated $Co(CO_3)_{0.5}(OH){\cdot}0.11H_2O$ microflower sample was dried at 60 ^oC for 24 h and subsequently annealed at 600 ^oC for 3 h with a heating rate of 5 ◦C min^{-1} to form Ag nanoparticles-decorated porous Co_3O_4 nanorods.

2.3. Instrument and characterization of the samples

Transmission electron microscopy (TEM) images and high-resolution TEM (HRTEM) images were measured on a JEOL and JEM 1230, respectively. Scanning electron microscopy (SEM) images were performed on a JSM-5300LV. Phases of the samples were characterized by X-ray diffraction (XRD, D8 Advance, Brucker, Germany) with a Cu-Kα line source (λ ~ 1.5406 Å). Infrared spectra were recorded using a Nicolet 6700 FTIR Spectrometer. Nitrogen adsorption/desorption isotherms of Ag nanoparticles-decorated porous Co_3O_4 nanorods were obtained using a Micromeritics at 77 K. The specific surface area (S_{BET}) of the samples was determined by the N_2 adsorption-desorption isotherm using the Brunauer–Emmett–Teller (BET) equation, and the desorption isotherm was used to determine pore size distribution using the Barret–Yoyner–Halender (BJH) method.

2.4. Gas sensing testing

The Ag nanoparticle-decorated $Co(CO_3)_{0.5}(OH){\cdot}0.11H_2O$ microflower precursors were dispersed in ethanol and then drop-casted onto an interdigitated electrode substrate using a micropipette. Thereafter, sensors were heat-treated at 600 ^oC for 3 h to obtain Ag nanoparticle-decorated porous Co_3O_4 nanorods as well as to increase adhesion between sensing materials and substrates. Gas sensing properties of nanocomposites were tested with several reduced gases including H_2, CO, C_2H_5OH and NH_3 at different operating temperatures (150 - 250 ^oC) using a homemade setup with high-speed switching gas flow (from/to air to/from balance gas). The air or target gases were directly exposed to the surface of the sensors through a quart tube at a constant flow rate of 200 sccm". Balance gases (0.1 % in air) were purchased from Air Liquid Group (Singapore). During sensing measurements, resistance of sensors was automatically

recorded through a Keithley controlled by a computer via a software program. Sensor response was calculated as $S = R_{gas}/R_{air}$, where R_{gas} and R_{air} are the form of sensor resistance in the presence of analytic gas and in air, respectively. The response time (τ_{resp}) and recovery time (τ_{recov}) were defined as the times required to achieve 90 % resistance to transformation when exposed to gas and air, respectively.

3. RESULTS AND DISCUSSION

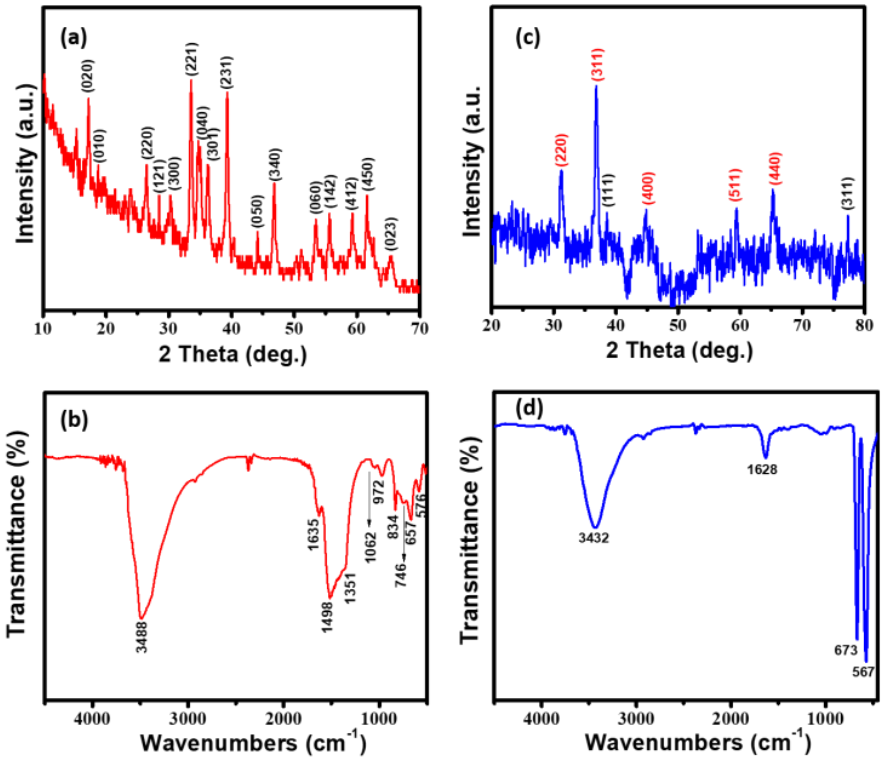

Figure 1. XRD pattern (a) and FTIR spectra (b) of Ag nanoparticles-decorated $Co(CO_3)_{0.5}(OH)\cdot 0.11H_2O$ mocroflowers; XRD pattern (c) and FTIR spectra (d) of Ag nanoparticles-decorated porous Co_3O_4 nanorods.

The phase purity and surface stages of as-synthesized nanomaterials were characterized by XRD and FTIR, as shown in Figure 1. For Ag nanoparticle-decorated $Co(CO_3)_{0.5}(OH)\cdot 0.11H_2O$ microflowers, the XRD patterns of the precursor sample correspond to typical diffraction peaks of orthorhombic $Co(CO_3)_{0.5}(OH)\cdot 0.11H_2O$ phase (JCPDS card No. 48-0083) (Figure 1a). Meanwhile, the FTIR of the sample (Figure 1b) shows bands at 1498, 834, 746, and 657 cm^{-1}, which may be related to the stretching vibrations of $\nu(OCO_2)$, $\delta(CO_3)$, $\delta(OCO)$, and $\rho(OCO)$, respectively. The peak at 1351 cm^{-1} is related to the symmetric stretching of $\nu_s(COO^-)$. The bands centered at 576 and 972 cm^{-1} are attributed to the vibrations of ρ_w(Co-OH) and δ(Co-OH), respectively. The broad band at 3488 cm^{-1} indicates the presence of water in the sample [16]. After the annealing process, the XRD pattern of the calcined sample shows that all peaks match well with the cubic spinel Co_3O_4 phase (JCPDS card No. 43-1003). Additionally, there are two diffraction peaks at 38.6° and 77.5° that are representative of the (111) and (311) planes of silver crystals [17]. The FTIR of the calcined sample indicates that these characteristic peaks of

$Co(CO_3)_{0.5}(OH)\cdot 0.11H_2O$ disappear, and in the meantime, two characteristic peaks of Co_3O_4 are clearly observed (Figure 1d). The band at 673 cm^{-1} originates from the stretching vibration mode of the tetrahedrally coordinated Co^{2+}– O bound, and the peak at 567 cm^{-1} is assigned to the octahedrally coordinated Co^{3+}– O bound [18]. Meanwhile, the bands at 1628 and 3432 cm^{-1} are attributed to the bending mode of the H–O–H and O-H of water in the sample [19]. These results confirm that Ag-decorated $Co(CO_3)_{0.5}(OH)\cdot 0.11H_2O$ was thoroughly transformed to Co_3O_4 with a great purity by annealing at 600 ^oC for 5 h.

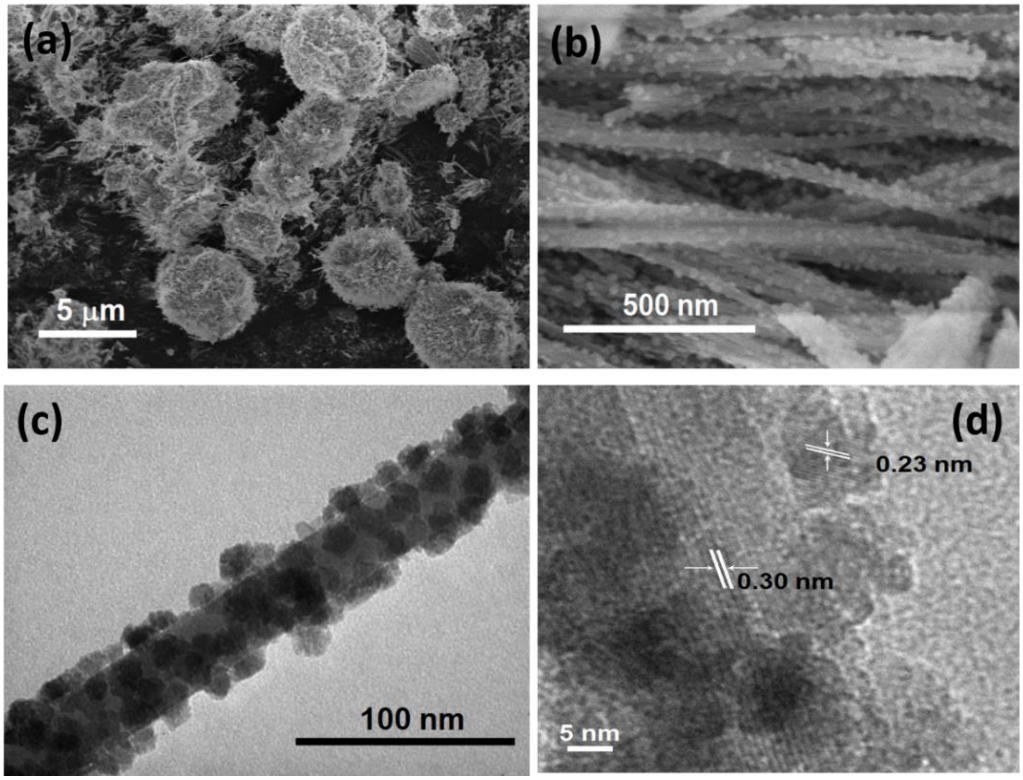

Figure 2. SEM images (a, b), TEM image (c) and HRTEM image (d) of Ag nanoparticles-decorated $Co(CO_3)_{0.5}(OH)\cdot 0.11H_2O$ microflowers.

To determine the morphology and structure of the precursor sample, the SEM, TEM and HRTEM analyses were performed and the results obtained are shown in Figure 2. The low magnification SEM image (Figure 2a) of Ag nanoparticle-decorated $Co(CO_3)_{0.5}(OH)\cdot 0.11H_2O$ composites shows that the sample consists of flower-like microstructures assembled by many nanorods. The length and diameter of a primary nanorod are about 2 μm and 30 nm, respectively. From the higher magnification SEM image (Figure 2b), uniform Ag nanoparticles with a size of ~ 10 nm decorated on the surface of cobalt carbonate hydroxide hydrate nanorods are clearly observed. The TEM image (Figure 2c) of the precursor sample further demonstrates that the Ag nanoparticles are homogeneously distributed on the surface of cobalt carbonate hydroxide hydrate nanorod. The HRTEM image of the sample (Figure 2d) reveals well-arranged lattice fringes with an interplanar spacing of 0.30 nm which corresponds well to the (300) crystal plane of $Co(CO_3)0.5(OH)0.11H_2O$, whereas the lattice spacing of 0.23 nm coincides with the (111) plane of Ag.

The morphology of the calcined sample changed significantly when compared to the Ag-decorated $Co(CO_3)0.5(OH)0.11H_2O$ precursor, as shown in Figure 3. The $Co(CO_3)0.5(OH)0.11H_2O$ flower-like microsphere architecture is broken, and the primary $Co(CO_3)0.5(OH)0.11H_2O$ nanorod precursor with a smooth surface are transferred into rough-surfaced porous Co_3O_4 nanorods (Figure 3a-b). At high temperatures, the phase transition from $Co(CO_3)0.5(OH)0.11H_2O$ to Co_3O_4 may cause the flower-like structure to collapse. The TEM image of an individual porous Co_3O_4 nanorod indicates that the nanorods are formed by interconnecting nanoparticles (Figure 3c).

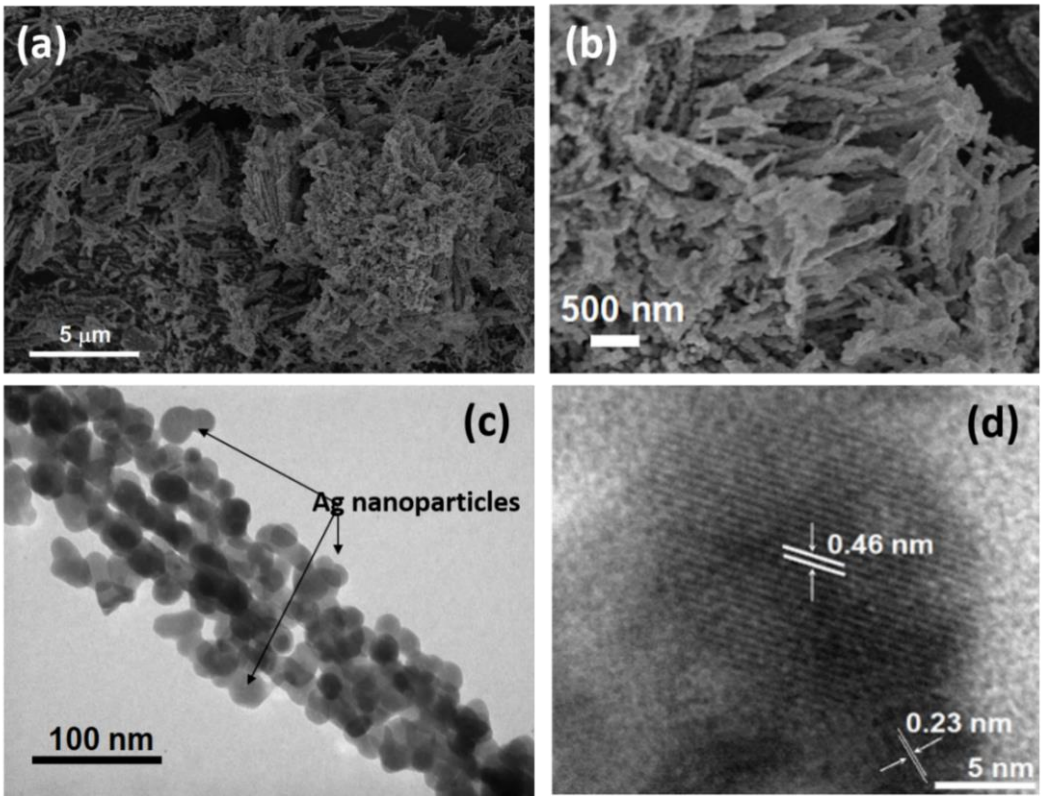

Figure 3. SEM images (a, b), TEM image (c) and HRTEM image (d) of Ag nanoparticles-decorated porous Co_3O_4 nanorods.

The average primary Co_3O_4 particle size is about 10 nm, which is the same particle size as Ag nanoparticles. So it is difficult to distinguish Co_3O_4 nanoparticles and Ag nanoparticles in a porous Co_3O_4 nanorod decorated Ag nanoparticles (Figure 3c). However, comparing the TEM image of the precursor (Figure 2c) with the TEM image of the calcined sample, the silver nanoparticles are the ones coated on the surface of porous nanorods, as shown in Figure 3c. As can be seen, the dark region and bright region in the TEM image confirm the formation of highly porous structures in an individual Ag-decorated Co_3O_4 nanorod. The HRTEM image (Figure 3d) of the sample clearly exhibits a lattice spacing of 0.46 nm that matches the (111) crystal plane of cubic spinel CO_3O_4 phase, whereas the lattice spacing of 0.23 nm corresponds to the (111) plane of metallic Ag. The formation mechanism of $Co(CO_3)0.5(OH)0.11H_2O$ microflowers, porous Co_3O_4 nanorods and Ag nanoparticles can be explained according to the following reactions [20, 21]:

$$CO(NH_2)_2 + 3H_2O \rightarrow 2NH_4^+ + CO_2 + 2OH^- \quad (1)$$

$$CO_2 + 2OH^- \rightarrow CO_3^{2-} + H_2O \quad (2)$$

$$Co^{2+} + 0.5\,CO_3^{2-} + OH^- \rightarrow Co(CO_3)_{0.5}(OH).0.11H_2O \quad (3)$$

$$3[Co(CO_3)_{0.5}(OH).0.11H_2O] + 0.39O_2 \rightarrow Co_3O_4 + 1.5CO_2 + 1.61\,H_2O \quad (4)$$

$$AgNO_3 + NaBH_4 \rightarrow Ag + \frac{1}{2}H_2 + \frac{1}{2}B_2H_6 + NaNO_3$$

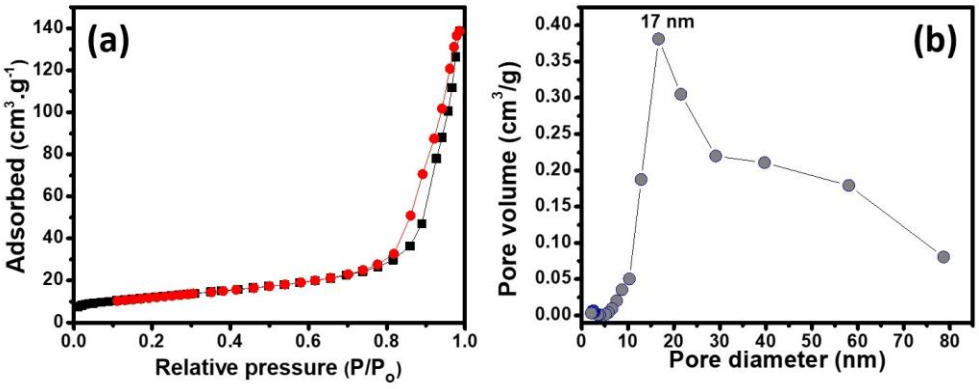

Figure 4. The nitrogen adsorption/desorption isotherms (a) and BJH pore size distribution profiles (b) of the Ag nanoparticle-decorated porous Co_3O_4 nanorods.

The highly porous architecture of Ag nanoparticle-decorated Co_3O_4 nanorods was further characterized by nitrogen adsorption–desorption isotherm (Figure 4). Figure 4a shows the N_2 adsorption-desorption isotherm of the sample, which indicates the H3 hysteresis loop with a type IV isotherm according to the IUPAC classification, demonstrating the presence of a mesoporous structure. Such a highly porous nanorod gives rise to a high BET specific surface area of 43 m^2/g. The BJH pore size distribution plot of as-synthesized Ag-decorated porous Co_3O_4 nanorods exhibits a pore size range of 3 - 80 nm and a maximum peak pore diameter of about 17 nm (Figure 4b). The highly porous structure of Ag-decorated Co_3O_4 nanorods can be attributed to the porosity of interparticles. As-fabricated porous Ag nanoparticle-decorated Co_3O_4 nanorods with a large surface area may favor their new gas sensing properties.

To evaluate the potential applicability in the gas sensing field of Ag nanoparticle-decorated porous Co_3O_4 nanorods, four reduced gases, including H_2, CO, C_2H_5OH and NH_3 were used. The H_2 gas sensing properties of the sensors are given in Figure 5, which shows the test results with various H_2 concentrations (25 - 500 pm) at different working temperatures to find out the optimized operating temperature. As shown in Figure 5(a-c), the sensors respond and recover quickly to H_2 gas at all working temperatures ranging from 150 to 250 ^oC. At 200 ^oC, the sensors exhibit the highest response to H_2 gas, which increases from 2.2 to 4.8 with an increment of the H_2 concentration from 25 to 500 ppm (Figure 5d). The influence of operating temperature on the H_2 response of the Ag nanoparticle-decorated porous Co_3O_4 nanorod sensor can be explained according to the kinetics and mechanism of gas adsorption and desorption on the sensor's surface. When the operating temperature is lower than the optimal temperature, chemical activation of sensing materials is weak, leading to a low response. By increasing the temperature, the optimal temperature can enhance the oxygen ionization and the reaction between oxygen species and hydrogen molecules, contributing to an increase in the response.

When the operating temperature is higher than the optimal working temperature, the adsorbed O_2 and H_2 molecules on the sensor's surface may quickly escape before their reaction, thus the response will decrease correspondingly [22]. Figure 5e shows the logarithm profile of the sensor response and H_2 concentration (25 - 500 ppm). The results show good linearity, indicating that Ag nanoparticle-decorated porous Co_3O_4 nanorods are promising sensing materials for detecting H_2 gas with a large dynamic range. Additionally, the sensors display rapid response and recovery times. At 200 ^oC, their response and recovery times for 500 ppm H_2 are 6 and 12 s, respectively (Figure 5f). Compared to other sensors, the sensor in this report shows higher response and faster response-recovery times (Table 1).

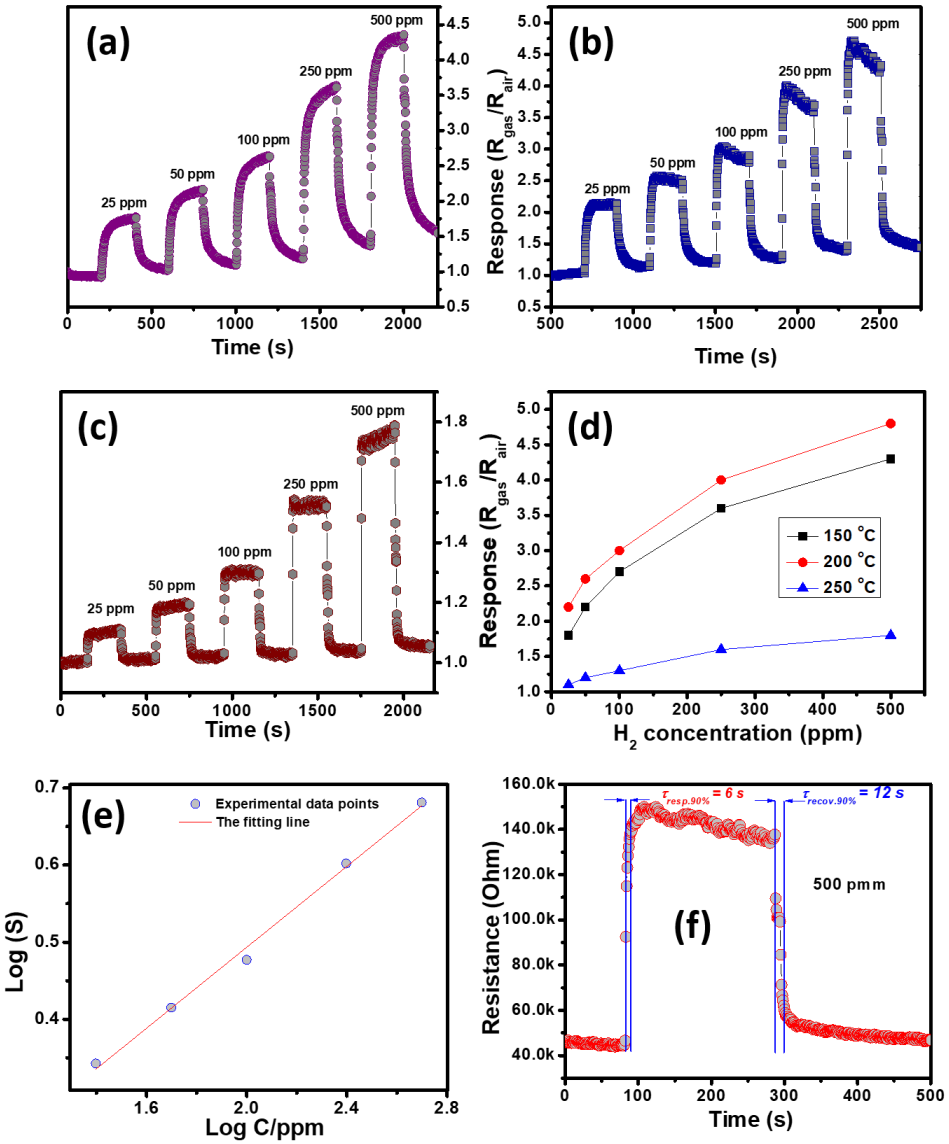

Figure 5. H_2 gas sensing properties of Ag nanoparticles-decorated porous Co_3O_4 nanorods sensors: Response transients to various H_2 concentrations at different working temperatures: (a) 150 ^oC, (b) 200 ^oC and (c) 250 ^oC; Response as a function of H_2 gas concentration (d); Relationship between sensitivity and H_2 concentration (e), and response-recovery times for 500 ppm H_2 at 200 ^oC (f).

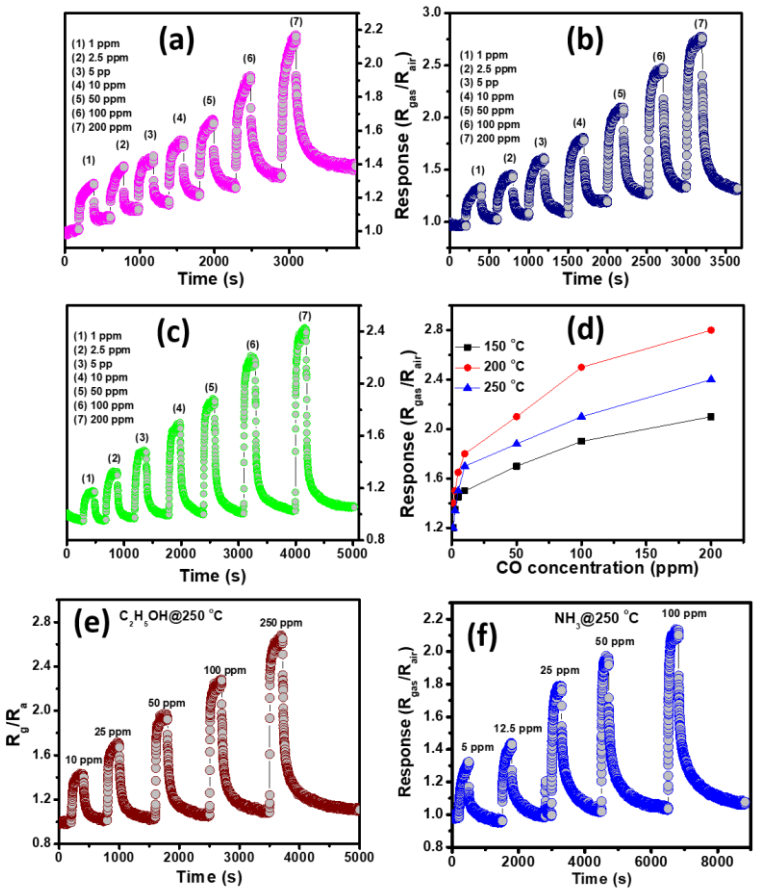

Figure 6. Response transients of Ag nanoparticles-decorated porous Co_3O_4 nanorods to CO (a-d), C_2H_5OH (e) and NH_3 (f).

Table 1. Comparison of hydrogen gas sensor performance with reported data.

Sensor	Optimal working temperature (^oC)	Concentration (ppm)	Response	Response-recovery times	Ref.
n-SnO_2/p-Co_3O_4 composite nanoparticles	350	500	4.5#	50 s - 435 s	[23]
Pd-capped CuO thin films	300	1000	$3.01^{\#}$	10 s - 50 s	[24]
Pd/SnO_2 nanoparticles	RT	1000	$1.2^{\#}$	214 s - 51.5 s	[25]
CuO nanorods	200	1000	4.5*	10 s - 16 s	[26]
ZnO hollow nanoparticles	225	100	89*	139 s - 2587 s	[27]
WO_3 thin film	250	100	87*	3 - 4 min - 8 - 9 min	[28]
Ag-decorated porous Co_3O_4 nanorods	200	500 100	$4.8^{\#}$ 230* 147*	6 s - 12 s	This work
$S^{\#} = R_g/R_a$ $S^* = (R_g\text{-}R_a)/R_a*100$					

The Ag nanoparticle-decorated porous Co_3O_4 nanorod sensors were also tested with CO, C_2H_5OH and NH_3 gases. Figure 6(a-d) presents the dynamic CO sensing graphs of the nanosensors as a function of CO concentration (1 - 200 ppm) at different operating temperatures. The Ag nanoparticle-decorated porous Co_3O_4-based sensors show the best detection of CO gas at 200 ^oC, which is similar to that of H_2 gas. At the optimal working temperature, their sensitivities increase from 1.4 to 2.8 with a range of CO concentration from 1 to 200 ppm; these values are lower than those of H_2 gas. The sensors also show insensitivity to C_2H_5OH and NH_3 gases, which increase slightly from 1.4 to 2.6 and from 1.3 to 2.1 for C_2H_5OH (10 - 250 ppm) and NH_3 (5 - 100 pm), respectively. The sensitivity of sensors to H_2 gas is significantly higher than that of other gases, which indicates that the Ag nanoparticles-decorated porous Co_3O_4 nanorods present good selectivity and potential as a candidate sensor for H_2 gas detection. The superior sensing performance of the Ag nanoparticle-decorated porous Co_3O_4 nanorods for H_2 over other gases is possibly due to the excellent catalytic feature of Ag nanoparticles, which promotes the dissociation of H_2 molecules into atoms, which is beneficial for the oxidation of H_2 molecular gas at low temperatures [29]. Furthermore, the highly porous Co_3O_4 nanorods have a large exposure of surface atoms, providing more active sites for the absorption of hydrogen molecules and hence promoting the surface reaction [30].

4. CONCLUSIONS

In summary, Ag nanoparticle-decorated porous Co_3O_4 nanorods were synthesized by a simple method using Ag nanoparticle-decorated $Co(CO_3)_{0.5}(OH)\cdot 0.11H_2O$ microflower precursors. The Co_3O_4 nanorods with a highly porous structure were assembled by many primary Co_3O_4 nanoparticles, and their surface was decorated by uniform Ag nanoparticles. The Ag nanoparticle-decorated porous Co_3O_4 nanorod-based sensors showed promising detection of H_2 gas with high response, good selectivity and fast response and recovery times. The combination of the excellent catalytic features of Ag nanoparticles and highly porous Co_3O_4 nanorods may be attributed to the enhanced H_2 gas sensing performance of the sensors.

Acknowledgements. This work was supported by the Vietnam National Foundation for Science and Technology Development (NAFOSTED) under grant number 103.02-2019.43.

CRediT authorship contribution statement. Vu Hung Sinh: Methodology, Investigation, Formal analysis, Writing – original draft. Duong Tuan Quang: Conceptualization, Formal analysis, Writing – original draft. Tran Quy Phuong: Methodology, Formal analysis. Tran Thai Hoa: Formal analysis, Supervision. Nguyen Van Hieu: Conceptualization, Formal analysis, Resources. Nguyen Duc Cuong: Conceptualization, Resources, Project administration, Funding acquisition, Writing – original draft.

Declaration of competing interest. The authors declare that they have no known competing financial interests or personal relationships that could have appeared to influence the work reported in this paper.

REFERENCES

1. Lee J. H. - Gas sensors using hierarchical and hollow oxide nanostructures: Overview, Sensors Actuators B Chem. **140** (2009) 319-336. https://doi.org/10.1016/ j.snb.2009.04.026.
2. Son L. L., Cuong D., Van Thi T., Hieu T. - Konjac glucomannan-templated synthesis of three-dimensional NiO nanostructures assembled from porous NiO nanoplates for gas sensors, RSC Adv. **9** (2019) 9584-9593. https://doi.org/10.1039/C9RA00285E.
3. Cheng P., Dang F., Wang Y., Gao J., Xu L., Wang C., Lv L., Li X., Zhang B., Liu B. -

Gas sensor towards n-butanol at low temperature detection: Hierarchical flower-like Ni-doped Co_3O_4 based on solvent-dependent synthesis, Sensors Actuators B Chem. **328** (2021) 129028. https://doi.org/10.1016/j.snb.2020.129028.

4. Sun J., Yang Y., Wang J., Zhang Z., Guo J. - In-situ construction of cobalt oxide/ nitrogen-doped porous carbon compounds as efficient bifunctional catalysts for oxygen electrode reactions, J. Alloys Compd. **827** (2020) 154308. https://doi.org/10.1016/ j.jallcom.2020.154308.
5. Wen Z., Zhu L., Mei W., Li Y., Hu L., Sun L., Wan W., Ye Z. - A facile fluorine-mediated hydrothermal route to controlled synthesis of rhombus-shaped Co_3O_4 nanorod arrays and their application in gas sensing, J. Mater. Chem. A. **1** (2013) 7511. https://doi.org/ 10.1039/c3ta11004d.
6. Geng B., Zhan F., Fang C., Yu N. - A facile coordination compound precursor route to controlled synthesis of Co_3O_4 nanostructures and their room-temperature gas sensing properties, J. Mater. Chem. **18** (2008) 4977. https://doi.org/10.1039/b805378b.
7. Nguyen H., El-Safty S. A. - Meso- and Macroporous Co_3O_4 Nanorods for Effective VOC Gas Sensors, J. Phys. Chem. C.**115** (2011) 8466-8474. https://doi.org/10.1021/jp1116189.
8. Han Y., Li H., Zhang M., Fu Y., Liu Y., Yang Y., Xu J., Geng Y., Wang L. - Self-supported $Co(CO_3)_{0.5}(OH)\cdot 0.11H_2O$ nanoneedles coated with $CoSe_2$-Ni_3Se_2 nanoparticles as highly active bifunctional electrocatalyst for overall water splitting, Appl. Surf. Sci. **495** (2019) 143606. https://doi.org/10.1016/j.apsusc.2019.143606.
9. Quang P. L., Cuong N. D., Hoa T. T., Long H. T., Hung C. M., Le D. T. T., Hieu N. V. - Simple post-synthesis of mesoporous p-type Co_3O_4 nanochains for enhanced H_2S gas sensing performance, Sensor. Actuat. B. **270** (2018) 158-166.
10. Cuong N. D., Tran T. D., Nguyen Q. T., Hai H. V. M., Hoa T. T., Quang D. T., Klysubun W., Tran P. D. - Highly porous Co-doped NiO nanorods: facile hydrothermal synthesis and electrocatalytic oxygen evolution properties, R. Soc. Open Sci. **8** (2021) 202352. https://doi.org/10.1098/rsos.202352.
11. Orfi H., A.A. Mekkaoui, B. Sündü, M. Laayati, S.A. Labyad, L. El Firdoussi, Ö. Metin, S. El Houssame, Ag, Co_3O_4, Ag–Co_3O_4, and Ag/Co_3O_4 Nanoparticles Decorated Mesoporous Natural Phosphate: Effect of Metal Synergy and Preparation Method on the Catalytic Reduction Reaction, J. Inorg. Organomet. Polym. Mater.,**32** (2022) 2192–2208. https://doi.org/10.1007/s10904-022-02262-8.
12. Zhu S., Tian Q., Wu G., Bian W., Sun N., Wang X., Li C., Zhang Y., Dou H., Gong C., Dong X., Sun J., An Y., Jing Q., Liu B. - Highly sensitive and stable H_2 gas sensor based on p-PdO-n-WO_3-heterostructure-homogeneously-dispersing thin film, Int. J. Hydrogen Energy. **47** (2022) 17821-17834. https://doi.org/10.1016/j.ijhydene.2022.03.237.
13. Meng X., Bi M., Xiao Q., Gao W. - Ultra-fast response and highly selectivity hydrogen gas sensor based on Pd/SnO_2 nanoparticles, Int. J. Hydrogen Energy. **47** (2022) 3157-3169. https://doi.org/10.1016/j.ijhydene.2021.10.201.
14. Chauhan P. S., Bhattacharya S. - Hydrogen gas sensing methods, materials, and approach to achieve parts per billion level detection: A review, Int. J. Hydrogen Energy. **44** (2019) 26076-26099. https://doi.org/10.1016/j.ijhydene.2019.08.052.
15. Li Z., Zhang G., Gao W., Zhao R., Wang Y. - Ag decorated ZnO nanocrystallines synthesized by a low-temperature solvothermal method and their application for high

response H_2 gas sensor, J. Mater. Sci. Mater. Electron. **30** (2019) 18959-18969. https://doi.org/10.1007/s10854-019-02253-5.

16. Son L. L., Van Thi T. T., Trung K. Q., Van Hieu N., Trung D. D., Cuong N. D. - Facile and Scalable Fabrication of Highly Porous Co_3O_4 and α-Fe_2O_3 Nanosheets and Their Catalytic Properties, J. Electron. Mater. **48** (2019) 7897-7905.
17. Pal N., Agarwal M., Gupta R. - Green synthesis of guar gum/Ag nanoparticles and their role in peel-off gel for enhanced antibacterial efficiency and optimization using RSM, Int. J. Biol. Macromol. **221** (2022) 665-678. https://doi.org/10.1016/j.ijbiomac.2022.09.036.
18. Zhou T., Lu P., Zhang Z., Wang Q., Umar A. - Perforated Co_3O_4 nanoneedles assembled in chrysanthemum-like Co_3O_4 structures for ultra-high sensitive hydrazine chemical sensor, Sensors Actuators B Chem. **235** (2016) 457-465. https://doi.org/10.1016/j.snb.2016.05.075.
19. Feng C., Yang J., Xiao C., Xin B., Zhang S., Wang L., Geng B. - Glycerate-derived Co_3O_4 nano-microspheres as efficient catalysts for oxygen evolution reaction, Appl. Surf. Sci. **598** (2022) 153795. https://doi.org/10.1016/j.apsusc.2022.153795.
20. Wang B., Zhu T., Bin Wu H., Xu R., Chen J. S., (David) Lou X.W. - Porous Co_3O_4 nanowires derived from long $Co(CO_3)_{0.5}(OH)\cdot 0.11H_2O$ nanowires with improved supercapacitive properties, Nanoscale. **4** (2012) 2145. https://doi.org/10.1039/c2nr11897a.
21. Mulfinger L., Solomon S. D., Bahadory M., Jeyarajasingam A. V., Rutkowsky S. A., Boritz C. -Synthesis and Study of Silver Nanoparticles, J. Chem. Educ. **84** (2007) 322. https://doi.org/10.1021/ed084p322.
22. Zhang L., Gao Z., Liu C., Zhang Y., Tu Z., Yang X., Yang F., Wen Z., Zhu L., Liu R., Li Y., Cui L. - Synthesis of TiO_2 decorated Co_3O_4 acicular nanowire arrays and their application as an ethanol sensor, J. Mater. Chem. A. **3** (2015) 2794-2801. https://doi.org/10.1039/C4TA06440B.
23. Yin X.T., Li J., Dastan D., Zhou W. D., Garmestani H., Alamgir F. M. - Ultra-high selectivity of H_2 over CO with a p-n nanojunction based gas sensors and its mechanism, Sensors Actuators B Chem. **319** (2020) 128330. https://doi.org/10.1016/j.snb.2020.128330.
24. Yadav P., Kumar A., Sanger A., Gautam Y. K., Singh B. P. - Sputter-Grown Pd-Capped CuO Thin Films for a Highly Sensitive and Selective Hydrogen Gas Sensor, J. Electron. Mater. **50** (2021) 192-200. https://doi.org/10.1007/s11664-020-08588-8.
25. Kadhim I. H., Hassan H. A., Abdullah Q. N. - Hydrogen Gas Sensor Based on Nanocrystalline SnO_2 Thin Film Grown on Bare Si Substrates, Nano-Micro Lett. **8** (2016) 20-28. https://doi.org/10.1007/s40820-015-0057-1.
26. Sarıca N., Alev O., Arslan L. Ç., Öztürk Z. Z. - Characterization and gas sensing performances of noble metals decorated CuO nanorods, Thin Solid Films. **685** (2019) 321-328. https://doi.org/10.1016/j.tsf.2019.06.046.
27. Nakate U. T., Ahmad R., Patil P., Bhat K. S., Wang Y., Mahmoudi T., Yu Y. T., Suh E., Hahn Y. B. - High response and low concentration hydrogen gas sensing properties using hollow ZnO particles transformed from polystyrene@ZnO core-shell structures, Int. J. Hydrogen Energy. **44** (2019) 15677-15688. https://doi.org/10.1016/j.ijhydene.2019.04.058.
28. Godbole R., Ameen S., Nakate U. T., Shaheer Akhtar M., Shin H. S. - Low temperature

HFCVD synthesis of tungsten oxide thin film for high response hydrogen gas sensor application, Mater. Lett. **254** (2019) 398-401. https://doi.org/10.1016/j.matlet.2019.07.110.

29. Cattabiani N., Baratto C., Zappa D., Comini E., Donarelli M., Ferroni M., Ponzoni A., Faglia G. - Tin Oxide Nanowires Decorated with Ag Nanoparticles for Visible Light-Enhanced Hydrogen Sensing at Room Temperature: Bridging Conductometric Gas Sensing and Plasmon-Driven Catalysis, J. Phys. Chem. C. **122** (2018) 5026-5031. https://doi.org/10.1021/acs.jpcc.7b09807.
30. MaJ., Mei L., Chen Y., Li Q., Wang T., Xu Z., Duan X., Zheng W. - α-Fe_2O_3 nanochains: ammonium acetate-based ionothermal synthesis and ultrasensitive sensors for low-ppm-level H_2S gas, Nanoscale. **5** (2013) 895-898. https://doi.org/10.1039/C2NR33201A.